

Dichromatic soliton-molecular compounds in synchronized mode-locked fiber lasers

Yudong Cui^{1,3,6,†,*}, Yusheng Zhang^{2,†}, Xiankun Yao⁴, Xiang Hao¹, Qing Yang¹, Daru Chen²,
Xueming Liu^{5,*}, Xu Liu^{1,3*}, and Boris Malomed^{7,8}

1 State Key Laboratory of Modern Optical Instrumentation, College of Optical Science and Engineering, Zhejiang University, Hangzhou 310027, China

2 Hangzhou Institute of Advanced Studies, Zhejiang Normal University, Hangzhou, China

3 ZJU-Hangzhou Global Scientific and Technological Innovation Center, No.733 Jianshe San Road, Xiaoshan District, Hangzhou, Zhejiang, China, 311200

4 School of Physics, Northwest University, 710127 Xi'an, People's Republic of China

5 School of automation, Nanjing University of Information Science & Technology, Nanjing 210044, China

6 Wuhan National Laboratory for Optoelectronics, Huazhong University of Science and Technology, Wuhan, 430074 China

7 Department of Physical Electronics, Faculty of Engineering, and Center for Light-Matter Interaction, Tel Aviv University, Tel Aviv 69978, Israel

8 Instituto de Alta Investigación, Universidad de Tarapacá Casilla 7D, Arica, Chile

†These authors contributed equally to this work

**Corresponding author e-mail: cuiyd@zju.edu.cn, liuxm@zju.edu.cn; liuxu@zju.edu.cn*

Abstract: Soliton molecules have been a striking research area, which is significant for the exploration of physical mechanism in various nonlinear systems, the analog to the molecule of matter, and the potential applications in multilevel encoding of optical communications. Here, we demonstrate a novel dichromatic soliton-molecular compound (SMC) that is a hybrid bound states of multiple pulses with two different frequencies connected by two different binding mechanisms. It exhibits unique temporal and spectral profiles that can be described as the bounded temporal and dichromatic soliton molecules. The vibrating SMCs are generated experimentally and numerically to demonstrate the intrinsic solution in the dissipative nonlinear system, which is characterized with the vibration both in time and frequency dimensions and dual-peak evolution trajectory induced by the time-frequency coupling. These results enrich the concept of soliton molecules and further promote the analogy to matter molecules.

1. Introduction

Solitons has been widely employed to reveal the evolution mechanism of fluids, Bose-Einstein condensates, plasmas, polymers, and optical systems, which indicates the intrinsic dynamics in nonlinear systems described by the nonlinear Schrodinger equation¹⁻³. In the past few decades, it has been extended to the context of dissipative solitons for the general case through allowing energy exchange with the environment^{4,5}. More complex and chaotic soliton behavior can be observed in these dissipative systems dominated by gain and loss⁵⁻⁹. Under interactions responsible for various emergent phenomena, solitons can be assembled to form bound states of increased complexity⁸⁻¹³. Particular wave-particle duality has led to intense research focusing on bound states, which presents striking analogies with the hierarchy of the atomic and molecular composition of matter¹²⁻¹⁵.

Temporal optical solitons circulating in mode-locked lasers produce the abundant cases for soliton formation, evolution and interaction^{4,14-20}. When two solitons with identical center frequencies form a bound state, the soliton molecules exhibit double-hump temporal intensity profiles and periodic spectral modulation patterns^{8,21}. Coherent interactions can form strong binding forces via the Kerr effect for the relatively small soliton separations with overlapping each other, and weak binding is expected under large pulse separation with long-range interactions, which may be attributed to dispersive wave, gain recovery, and acousto-optic mechanisms^{14,15,22-25}. Nonlinear dissipative conditions enable various nonlinear dynamics of bound solitons, such as exceptional points, attractors, and bifurcation^{5,20,26,27}. In recent years, the oscillation and vibration dynamics of soliton molecules have been observed with the assist of the real-time spectroscopy, booming the related studies as it provides a vivid expression at the point of the analog to the molecule of matter^{4,14,26,28}. Optical supramolecular structures and soliton complexes and crystals were illustrated under the interaction of multiple solitons^{9,15,25,26,29}.

One of the prototypical excitations of soliton molecules is to explore how far the analog with matter molecules could be developed^{15,26}. However, the reported soliton molecules in mode-locked lasers generally consist of almost several identical solitons owing to the energy quantization and gain competition effect³⁰, which interact through the same binding mechanism, although solitons of different polarizations or wavelengths and multicomponent spatial solitons have been discovered as co-propagating bound states^{12,14,31-33}. Considering the diversity of

molecular constitutions, there should be more studies on soliton molecules. Recently, polychromatic soliton molecules, which are under a bound state in frequency domain, have been realized theoretically and experimentally in mode-locked fiber lasers with soliton trapping dynamics via cross-phase modulation (XPM) and can be used to manipulate the emitting pulse profiles³⁴⁻³⁶. This paves the way for soliton molecular compounds containing multiple elementary soliton molecules of different dimensions, which has not been reported.

In this study, we developed the temporal dichromatic soliton molecular compound (SMC) in a synchronous mode-locked fiber laser, which is composed of multiple optical solitons with two different frequencies illustrating the diverse hybrid bound states under the balance of different binding forces. The change of pump power and delay time would produce the periodical operation state that indicates the vibration of SMC. A numerical simulation was also implemented with the coupled nonlinear Schrödinger equation (cNLSE) to consider the XPM effect. The periodical solution can be obtained theoretically with appropriate gain and delay, which should be the intrinsic vibration state of SMC originating from the nonlinear dynamics of the dissipative system, just as the reported vibration of temporal soliton molecule (TSM) [4][14]. These results provide a way to realize complex structure soliton molecules in multiple dimensions, which can further promote the analogy with molecules.

2. Principle and experimental setup

Figure 1(a) illustrates the characterizations of the SMC in the time-frequency space where the typical features of TSM and dichromatic soliton molecule (DSM) can be both observed. For example, when one soliton of TSM is bonded with a soliton at another wavelength, SMC is formed with the structure of 2+1. So the TSM can be identified by the spectrum with interference fringes, and the spectrum at another wavelength is smooth, as shown in the projections to panels I of Fig. 1(a). On the other hand, the interference fringes can be also observed on the temporal profile in the projections to panels II of Fig. 1(a) indicating the existence of DSM that two solitons with different wavelengths overlap completely in time³⁴. The two overlapped solitons of DSM produce the remarkable XPM effect that induces the trapping potential forcing the same propagation velocity for two different colored solitons. The two separated pulses of TSM can also maintain the same velocity which is bonded via the long-range interaction, so that the

co-propagation hybrid three-body bound state is formed under the balance of two different binding forces. For the case of 2+2 SMC, there are two TSMs at two frequencies. If the two pulses of one TSM are both trapped by the other TSM, all the spectra and temporal profiles of the 2+2 SMC have periodic interference fringes, which can be seen in projection panels III and IV of Fig. 1(a). However, the other structure of 1-2-1 or 1-1-2 may be possible when the pulse separations of two TSMs are different. The results would demonstrate a new kind of soliton bound state that is analog to the more complex molecule compound which would be made up of multiple bonds or atoms, such as CaC_2 or NaOH . Additionally, it is helpful to deepen the understanding of the complex nonlinear system and interaction. Further, other distinct types of soliton compounds can be deviated according to the soliton numbers at two frequencies, such as 3+3, 4+2 and even $M+N$ SMC. Here M and N are the positive integer. It means the balance of the bound state with the arbitrary number of solitons at two wavelengths, as the gain competition has been circumvented largely.

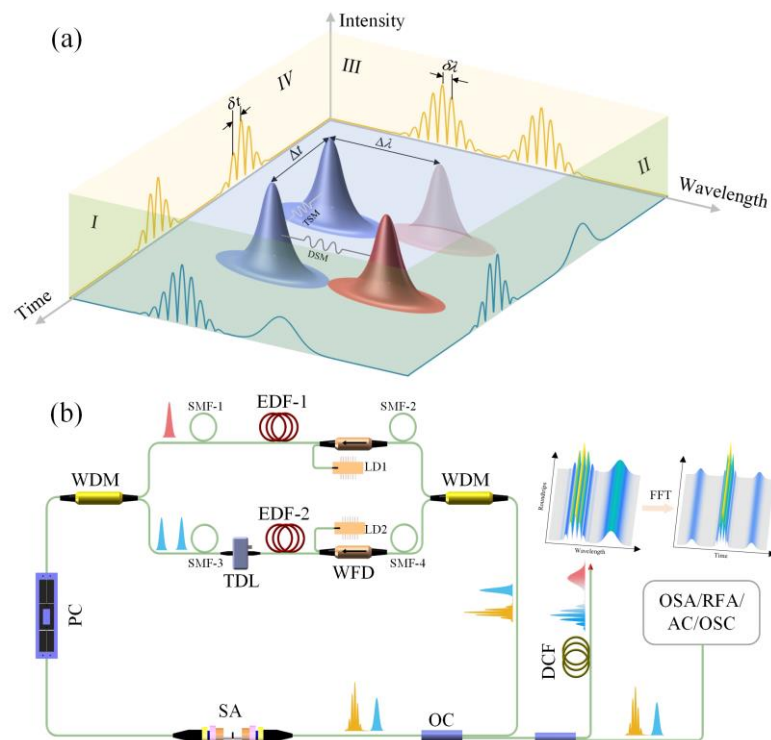


Figure 1. (a) Conceptual illustration of SMC. Pulses with red and blue colors correspond to the two frequencies that are trapped via XPM. When the light-red pulse is absent, the illustration describes the 2+1 SMC, and all the four pulses can model 2+2 SMC. Panel-I: spectrum of 2+1 SMC; Panel-II: temporal profile of 2+1 SMC; Panel-III: spectrum of 2+2 SMC; Panel-IV: temporal profile of 2+2 SMC. The time separation Δt and spectral modulation period $\delta\nu$ (or $\delta\lambda$) for

TSM have an inverse relationship, $\Delta t = 1/\delta\nu$. The frequency separation $\Delta\nu$ (or $\Delta\lambda$) and temporal modulation period δt for DSM are also reciprocal, $\Delta\nu = 1/\delta t$. (b) Experimental setup for generating and investigating the SMC. The spectral evolution and autocorrelation traces with respect to roundtrip (RT) can be obtained.

The experimental setup is shown in Fig. 1(b). Here, SMCs were generated in a mode-locked fiber laser with two branches to compensate the dispersion-induced time delay of solitons with different wavelengths. Similar systems have been utilized to achieve dual-comb lasers, synchronized multi-wavelength pulses, and simultaneous generation of polytype solitons, which have potential applications in coherent combination, laser ranging, and ultrafast transient spectroscopy³⁷⁻⁴¹. Two 1550/1570 wavelength division multiplexers (WDMs) were used to fabricate two branches of the signals at 1550 nm and 1570 nm, respectively. The operation bandwidth of the WDM at the two wavelengths was 20 nm. Each branch includes a section of erbium-doped fiber (EDF) to avoid gain competition, and a multifunctional device (MFD) used as a 980/1550 WDM and an isolator. EDF-1 for the generation of pulses at 1550 nm was 3.8 m and EDF-2 for 1570 nm was 4.5 m. A time delay line (TDL) was used in the 1550 nm branch to precisely adjust the dispersion-induced delay difference. The signals at the two branches were combined and passed through a common saturable absorber (SA) and coupler (OC) with an output ratio of 20%. A polarization controller (PC) was used to optimize the soliton operation. The SA is a home-made transmission-type mode locker based on single-walled carbon nanotube. The total length of the laser cavity was ~10.7 m. The lengths of SMF-1, SMF-2, SMF-3, and SMF-4 are 2.2, 2, 1.5, and 2 m, respectively. The length of common fiber is 2.7 m. The net dispersion conditions for the 1550 nm and 1570 nm branches were -0.073ps^2 and -0.044ps^2 , respectively. The emitted pulses were monitored by an optical spectrum analyzer (OSA), autocorrelator (AC), radio frequency analyzer (RFA), and a high-speed real-time oscilloscope (OSC). The real-time spectra were recorded by temporally stretching the solitons in a 10-km-long dispersion-compensating fiber (DCF) with a dispersion of -160ps/nm/km , which is called the dispersive Fourier transform (DFT) technique.

The temporal evolution process during the generation and measurement of the SMC is shown in Fig. 1(b). Pulses at 1550 nm and 1570 nm were transmitted independently in two branches and were combined by the 1550/1570 WDM to form the SMC, where the interference fringe on the

temporal profiles indicates the synchronous propagation of DSM. After outputting, SMC passes through the dispersion medium, and the spectra map to the temporal domain^{16,42}. However, it is inapplicable for asynchronous dual-wavelength solitons because the relative temporal position of two solitons with different frequencies changes along with time⁴³. The typical DSM can be achieved by finely tuning the time delay line (TDL) with suitable pump powers (see Figs. S1 and S2 in the Supplementary Material and Video S1 for details). The spectral evolution, pulse train, and radio frequency confirm a stable DSM operation.

3. Results

With suitable pump powers and slightly adjusting TDL, 2+1 SMC can be obtained in Fig. 2. The real-time spectral dynamics is shown in Fig. 2(a), where there is a TSM at 1550 nm and a single soliton at 1570 nm. The parallel evolution pattern for solitons at two wavelengths in Fig. 2(a) implies the synchronized transmission of the three solitons. This indicates that two solitons at 1550 nm is trapped by one soliton at 1570 nm, although one soliton at 1550 nm do not interact directly with 1570 nm soliton, revealing the strong binding force between the TSMs that can drive the motion of the soliton. The asymmetrical spectral profile can be attributed to the third-order dispersion in 1550/1570 WDM⁴⁴. The corresponding autocorrelation traces, which are the Fourier transformation of single-shot spectrum of Fig. 2(b) according to the Wiener-Khinchin theorem⁴⁵, are shown in Fig. 2(c). A unique double structure can be observed, where the evenly spaced sharp peaks on the central metaenvelope indicate the temporal interference of DSM and the three-hump profile originates from TSM. The autocorrelation trace measured in experiment was shown in Fig. S1 in the Supplementary Material, exhibiting the similar features. The interval between the central sharp peaks of $\delta t=0.36$ ps corresponds to the wavelength separation of $\Delta\lambda\sim 22$ nm. The spectral modulation period $\delta\lambda=3.95$ nm in Fig. 2(b) corresponds to the hump separation of $\Delta t=2.03$ ps for TSM in Fig. 2(c). The spectral and energy evolution in Fig. 2(a) implies that the 2+1 SMC is stable. The uniform pulse train measured directly by the oscilloscope and RF spectrum with a signal-to-noise ratio >60 dB in Fig. 2(d) further verifies the stable SMC operation. The fundamental frequency was obtained as ~ 19.1455 MHz and the corresponding roundtrip time was ~ 52.23 ns. The 2+1 SMC with different separations can also be obtained by adjusting the intracavity PC and TDL. The optical spectra with $\delta\lambda=0.7$ nm, 1.31 nm and 2.82 nm are displayed in Fig. 2(e), corresponding to time separations Δt of soliton molecules of 11.6 ps, 6.2 ps, and 2.9 ps, respectively. The 2+1 SMC represents a particular hybrid soliton bound state. The distinct

soliton number and optical power at two wavelengths can be realized when the gain competition is largely suppressed.

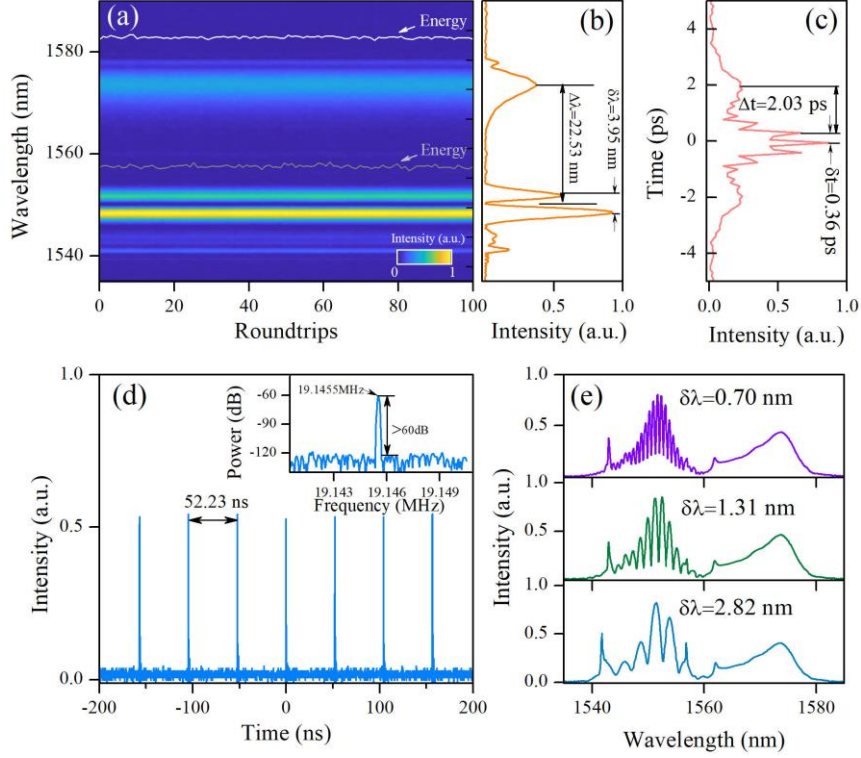


Figure 2. Characterizations of the 2+1 SMC. (a) Real-time spectral evolution measured using DFT. The energy evolution of pulses at 1550 nm and 1570 nm are the grey and white lines, respectively. (b) Single-shot spectrum corresponding to the last frame of (a). (c) Autocorrelation traces calculated via the Fourier transform of single-shot spectrum in (b). (d) Pulse train measured directly by OSC. Inset: Fundamental RF spectrum with the range of 10 kHz. (e) Optical spectra of 2+1 SMC for three other cases measured by OSA.

Further slightly increasing the pump power and adjusting the delay line and polarization, the periodical spectral evolution of 2+1 SMC can be observed, as shown in Fig. 3(a). 2+1 SMC is a three-body structure connected by two types of binding forces whose variation drives the periodic motion of solitons. The oscillating phase (ϕ_1) and pulse separation (Δt_1) of the TSM at 1550 nm were extracted with the methods in Ref. [46], as shown in Fig. 3(b). It is a kind of vibrating TSM with the pulse separation varying from 1.89 ps to 2.15 ps with the period of ~ 33 roundtrips^{4,14}. However, the dual-peak structure can be seen in one period, which should be attributed to the

interaction with the soliton at another wavelength. The coupling between two oscillating solitons results in the nonlinear dynamics to double the oscillation frequency. On the other hand, the spectral centroids (λ_c) as the center wavelength were calculated (see Supplementary Material) and the wavelength separation can be obtained, as shown in Fig. 3(c). The separation changes from 23.6 nm to 24.5 nm, indicating the vibration of DSM at the dimension of wavelength. The variation of wavelength can be induced by XPM, the binding force between DSM, corresponding to the change of the relative position. As it also would be influenced by feature of soliton at each wavelength (vibration of TSM), the dual-peak periodical oscillation is produced in Fig. 3(c) demonstrating the coupling between time and frequency domain.

The vibration process of 2+2 SMC were also recorded experimentally and shown in Fig. 3(d), when the pump power for 1570 nm is increased. The interference fringes can be both seen on the spectra at 1550 nm and 1570 nm. The spectra at two wavelengths follow the time-spectrum mapping relation, indicating the intrinsic bound states of the four solitons with the identical velocities. The TSM at 1550 nm display the oscillating separation and relative phase in Fig. 3(e), while TSM at 1570 nm possesses the oscillating separation and the slipping phase in Fig. 3(f). And the frequency doubling (dual-peak structure) can be seen for the evolution of temporal separation at 1570 nm, which implies the interaction among 2+2 SMC. The separations of the calculated averaged center wavelengths (spectral centroids) of TSMs also show the oscillation evolution. However, the evolution trajectory obviously contains several frequency components implying the complex interaction process for the four-body SMC. As the pulse separations for two TSMs are similar, the four solitons may be organized as 2-2 like that in Fig. 1(a). However, since the soliton features at two wavelengths are different, the intrinsic pulse separation of TSM should be different. As a result, the SMC tends to be broken by the unbalanced forces after thousands of the roundtrips, so that the stable 2+2 SMC can only be observed momentarily in experiment. In comparison with the reported soliton molecular complexes^{15,26}, SMC shows a distinct motion dynamic under two types of binding forces, in addition to the different spectral and temporal features. The vibration at two dimensions of time and frequency and the nonlinear dynamics induced by the time-frequency coupling should be the typical features of SMC.

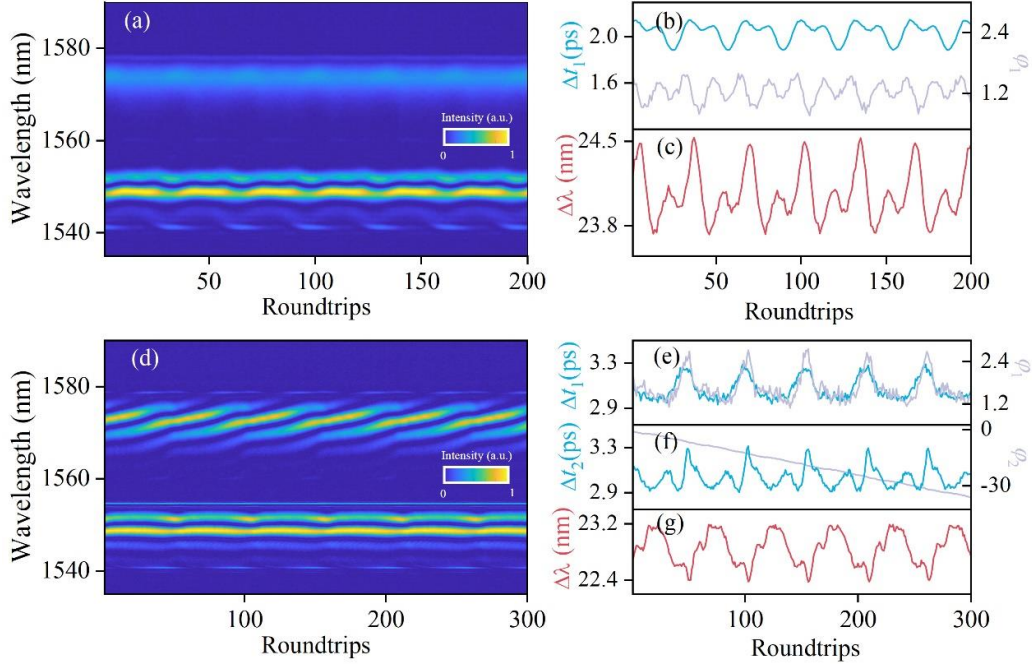


Figure 3. Vibration evolution of SMC. (a) Real-time spectral evolution of 2+1 SMC measured using DFT. (b) Evolution of the temporal separation and relative phase of TSM at 1550 nm. (c) Evolution of wavelength separation ($\Delta\lambda$) between two wavelengths. (d) Real-time spectral evolution of 2+2 SMC. Evolution of the temporal separation and relative phase of TSMs at (e) 1550 nm and (f) 1570 nm. (g) Evolution of wavelength separation ($\Delta\lambda$) between two wavelengths.

The existence of SMC can be further verified by numerical simulations. The model is established according to the experimental setup in Fig. 1(b) described with the round-trip model to consider every action of the components, and the parameters match the experimental conditions. The Ginzburg-Landau equation (GLE) is used to describe the pulse propagation in optical fibers [1,26]:

$$\frac{\partial u}{\partial z} = \frac{g}{2}u - i\frac{\beta_2}{2}\frac{\partial^2 u}{\partial t^2} + i\gamma|u|^2u + \frac{g}{2\Omega_g^2}\frac{\partial^2 u}{\partial t^2}, \quad (\text{S4})$$

where t and z are the time and propagation distances, respectively, u denotes the normalized slowly varying envelope of pulses, and β_2 and γ are denoted as the second-order dispersion coefficient and cubic refractive nonlinearity of the fiber, respectively. For the gain fiber EDF, the gain spectrum bandwidth is Ω_g , and the gain saturation is expressed as $g=g_0\exp(-E_p/E_s)$, where E_p is the pulse energy, and g_0 and E_s are the small-signal gain coefficient and gain saturation energy,

respectively. For the SMF, $g = 0$. To describe the propagation of DSM in fibers, the coupled nonlinear Schrödinger equation (cNLSE) is employed to consider the XPM effect [1]:

$$\frac{\partial u_1}{\partial z} = -\frac{1}{v_{g1}} \frac{\partial u_1}{\partial t} - i \frac{\beta_2}{2} \frac{\partial^2 u_1}{\partial t^2} + i\gamma \left(|u_1|^2 + 2|u_2|^2 \right) u_1, \quad (\text{S5a})$$

$$\frac{\partial u_2}{\partial z} = -\frac{1}{v_{g2}} \frac{\partial u_2}{\partial t} - i \frac{\beta_2}{2} \frac{\partial^2 u_2}{\partial t^2} + i\gamma \left(|u_2|^2 + 2|u_1|^2 \right) u_2. \quad (\text{S5b})$$

u_1 and u_2 denote the normalized slowly varying envelopes of pulses at 1550 nm and 1570 nm, respectively. β_2 and γ are denoted as the dispersion coefficient and cubic refractive nonlinearity of the fiber, respectively. v_{g1} and v_{g2} are the group velocities at two wavelengths whose relative difference can be attributed to the dispersion terms because the two wavelengths are close. Consequently, the group velocity terms can be ignored. The SA is modeled with a transfer function with a transmission of $T=1-\alpha_0/(1+P/P_{\text{sat}})$, where α_0 is the unsaturated loss, α is the modulation depth, P is the instantaneous pulse power, and P_{sat} is the saturation power. Because the carbon nanotube is a type of slow saturable absorber, the intensity of the DSM is expressed as $u=|u_1|+|u_2|$. The effect of the TDL can be included by multiplying the phase delay $u_1=u_1\exp(i\omega t_D)$, where ω is the angular frequency, and t_D is the relative time delay between the two branches. The 1550/1570 WDM is composed of two bandpass filters with the transfer function expressed as

$$F_{1,2} = \exp\left(-\frac{1}{2} \left[\frac{(\omega - \omega_{1,2})}{\Delta\omega_{1,2}} \right]^8\right) \quad (\text{S6})$$

Where $\omega_{1,2}$ is the center frequency corresponding to solitons at two wavelengths and $\Delta\omega_{1,2}$ is the bandwidth (1/e) of the filters. The initial input pulse for our simulation was a very weak pulse with a Gaussian profile. We used the following parameters in our simulation model to obtain SMC, which guided our experiments: $g_0=3$ dB/m, $\Omega_g=40$ nm, $\gamma=4.5$ W⁻¹ km⁻¹, $\beta_2=20$ ps²/km for EDF-1 and $\beta_2=23.6$ ps²/km for EDF-2; $\gamma=1.3$ W⁻¹ km⁻¹ and $\beta_2=-21.6$ ps²/km for SMF; $\lambda=1550$ nm, $c=3\times 10^8$ m/s, $t_D=-0.355$ ps for 2+1 SMC and $t_D=-0.31$ ps for 2+2 SMC; $\alpha_0=0.2$, $P_{\text{sat}}=30$ W. The length of SMF and EDF is as that in the experiment setup.

When $E_s = 26$ pJ at 1550 nm and $E_s = 3$ pJ at 1570 nm, the stable 2+1 SMC was generated in Fig. 4, which agrees well with the experimental results in Fig. 2. The detailed formation dynamics can be seen in Supplementary Video S2. Fig. 4(a) shows the optical spectrum of the 2+1 SMC obtained from the simulation, and Fig. 4(b) exhibits the corresponding temporal profile, where one

pulse at 1550 nm and one at 1570 nm overlap completely in time, which forms the metaenvelope with the interference fringes like that in Fig. 1(a). It should be noted that the autocorrelation function of the pulse intensity in Fig. 4(b) corresponds to the results in Fig. 2(d). By increasing E_s for 1550 nm to 30 pJ, the vibrating 2+1 SMC can be obtained. It shows the periodically spectral evolution in Fig. 4(c), and the corresponding temporal evolution in Fig. 4(d) exhibits the vibration of 2+1 SMC clearly. The evolutions of the extracted temporal and wavelength separation in Figs. 4(e) and 4(f) have the oscillation behavior and dual-peak structure, which is similar to that in Figs. 3(b) and 3(c). The typical features of 2+1 SMC are illustrated in simulation. When the saturation energy for 1570 nm is set as 16 pJ, the similar evolution process with Fig. 3(d) can be produced, as shown in Fig. 5(a) where the vibrating 2+2 SMC contains the TSM at 1550 nm with oscillating phase and TSM at 1570 nm with the slipping phase. The temporal evolution can be seen in Supplemental Material. The evolutions of temporal and wavelength separation in Figs. 5(b) 5(c) and 5(d) also agree well with the experimental results (Figs. 3(e), 3(f) and 3(g)). Since the cavity parameters can be adjusted precisely in simulation, the generation of 2+2 SMC can be controlled from the stable to vibrating state.

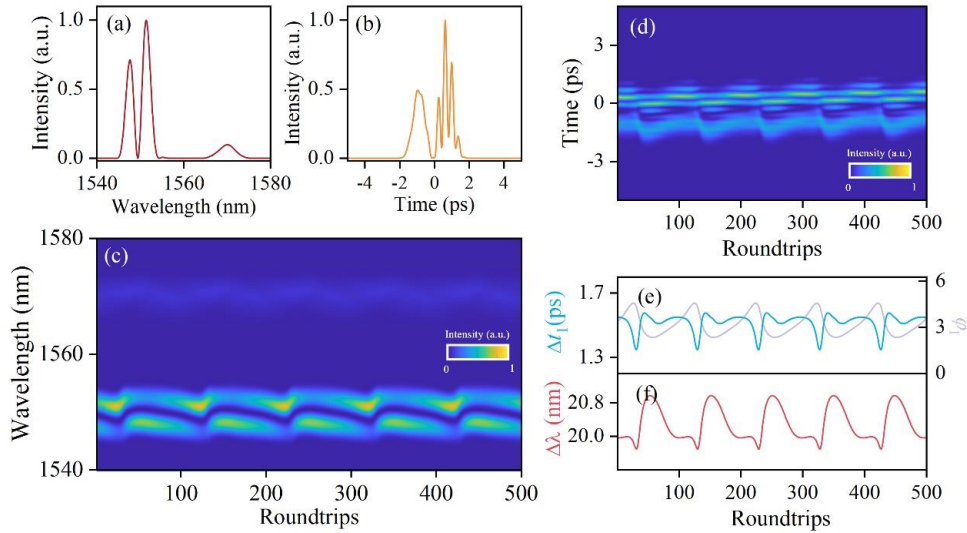


Fig. 4. Simulation results of 2+1 SMC. (a) Optical spectrum and (b) temporal profile of stable 2+1SMC. (c) Spectral evolution of vibrating 2+1 SMC with respect to roundtrips. (d) Evolution of pulse with respect to roundtrips. (e) Evolution of the temporal separation and relative phase of TSM at 1550 nm. (f) Evolution of wavelength separation.

The simulation model is a coupled nonlinear dissipative system based on GLE and cNLSE. The simulation results verify the existence of the stable SMC and indicate that the vibrating SMC is the intrinsic solution of the nonlinear system. However, there are obvious difference between experimental and simulation results, such as the evolution of phase and oscillation period. Many factors are not included in simulation, such as the variation of gain coefficient, high-order dispersion and nonlinearity. In this work, only 2+1 and 2+2 SMC are presented, but the conception can be extended to the wider range. For example, more pulses can be generated for each wavelength to form the more complicated SMC, and the harmonic operation can be also obtained under long range interaction. Moreover, by utilizing the dense WDM, solitons can be generated at tens of wavelengths simultaneously and the soliton number and soliton features can be also chosen flexibly.

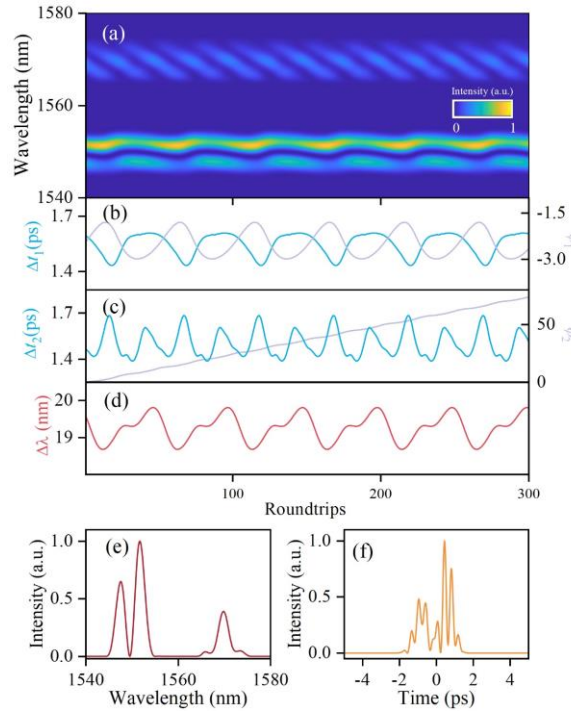


Fig. 5. Simulation results of 2+2 SMC. (a) Spectral evolution of vibrating 2+2 SMC. Evolution of the temporal separation and relative phase of TSMs at (b) 1550 nm and (c) 1570 nm. (d) Evolution of wavelength separation ($\Delta\lambda$) between two wavelengths.

4. Conclusion

SMC, as a combination of TSM and DSM, was generated and investigated in a synchronously mode-locked fiber laser. Multiple pulses with two different wavelengths were

bounded and propagated with the same velocity, and 2+1 SMCs was obtained when the gain competition is suppressed. The temporal and spectral features are completely different from the reported soliton molecule and complexes []. The vibration of 2+1 and 2+2 SMC was also observed experimentally by increasing the pump powers and they show the periodical oscillation for temporal and wavelength separations. The internal interaction of SMC induces the frequency-doubling phenomenon during the vibration process. The numerical model is established to verify the generation of SMC, and the vibration state can be also obtained with appropriate saturation energy, which exhibits the similar features with the experimental results.

Acknowledgements

The authors acknowledge support from the National Natural Science Foundation of China under Grant Agreements 61705193, 61525505, 11774310, and 62035010, the Natural Science Foundation of Zhejiang Province under Grant Nos. LGG20F050002 and LY19F050014, the Open Project Program of Wuhan National Laboratory for Optoelectronics No. 2020WNLOKF008, and the Independently Project by Zhejiang Normal University under Grant No. 2021ZS05.

References

1. G. P. Agrawal, *Nonlinear Fiber Optics* (Academic Press, 2007).
2. J. Denschlag et al., “Generating solitons by phase engineering of a Bose-Einstein condensate,” *Science* **287**(5450), 97–101 (2000).
3. Thierry Dauxois and Michel Peyrard, *Physics of Solitons* (Cambridge University Press, 2005).
4. K. Krupa et al., “Real-Time Observation of Internal Motion within Ultrafast Dissipative Optical Soliton Molecules,” *Phys. Rev. Lett.* **118**(24), 243901 (2017).
5. M. Marconi et al., “Vectorial dissipative solitons in vertical-cavity surface-emitting lasers with delays,” *Nat. Photon.* **9**(7), 450–455 (2015).
6. J. M. Dudley, F. Dias, M. Erkintalo, and G. Genty, “Instabilities, breathers and rogue waves in optics,” *Nat. Photon.* **8**(10), 755–764 (2014).
7. J. M. Soto-Crespo and N. Akhmediev, “Soliton as strange attractor: Nonlinear synchronization and chaos,” *Phys. Rev. Lett.* **95**(2), 024101 (2005).
8. B. A. Malomed, “Bound solitons in the nonlinear Schrödinger-Ginzburg-Landau equation,” *Phys. Rev. A* **44**(10), 6954–6957 (1991).
9. D. C. Cole et al., “Soliton crystals in Kerr resonators,” *Nat. Photon.* **11**(10), 671–676 (2017).
10. F. Kurtz, C. Ropers, and G. Herink, “Resonant excitation and all-optical switching of femtosecond soliton molecules,” *Nat. Photon.* **14**(1), 9–13 (2020).
11. C. Becker et al., “Oscillations and interactions of dark and dark–bright solitons in Bose–Einstein condensates,” *Nat. Phys.* **4**(6), 496–501 (2008).

12. G. I. Stegeman and M. Segev, "Optical Spatial Solitons and Their Interactions: Universality and Diversity," *Science* **286**(5444), 1518–1523 (1999).
13. A. Leitenstorfer et al., "Soliton molecules in femtosecond fiber lasers: universal binding mechanism and direct electronic control," *Optica* **8**(10), 1334–1339 (2021).
14. G. Herink et al., "Real-time spectral interferometry probes the internal dynamics of femtosecond soliton molecules," *Science* **356**(6333), 50–54 (2017).
15. W. He et al., "Formation of optical supramolecular structures in a fibre laser by tailoring long-range soliton interactions," *Nat. Commun.* **10**(1), 5756 (2019).
16. X. Liu, X. Yao, and Y. Cui, "Real-Time Observation of the Buildup of Soliton Molecules," *Phys. Rev. Lett.* **121**(2), 023905 (2018).
17. Y. Song et al., "Attosecond timing jitter within a temporal soliton molecule," *Optica* **7**(11), 1531–1534 (2020).
18. Y.-E. Wang et al., "Vortex soliton molecule in a fiber laser," *Opt. Express* **28**(7), 9666–9676 (2020).
19. L. G. Wright et al., "Mechanisms of spatiotemporal mode-locking," *Nat. Phys.* **16**565–570 (2020).
20. S. V Sergeev, C. Mou, A. Rozhin, and S. K. Turitsyn, "Vector solitons with locked and precessing states of polarization," *Opt. Express* **20**(24), 27434–27440 (2012).
21. M. Stratmann, T. Pagel, and F. Mitschke, "Experimental observation of temporal soliton molecules," *Phys. Rev. Lett.* **95**(14), 143902 (2005).
22. A. Komarov, K. Komarov, and F. Sanchez, "Quantization of binding energy of structural solitons in passive mode-locked fiber lasers," *Phys. Rev. A* **79**(3), 033807 (2009).
23. A. Hause, H. Hartwig, M. Böhm, and F. Mitschke, "Binding mechanism of temporal soliton molecules," *Phys. Rev. A* **78**(6), 063817 (2008).
24. E. M. Dianov, A. V. Luchnikov, A. N. Pilipetskii, and A. M. Prokhorov, "Long-range interaction of picosecond solitons through excitation of acoustic waves in optical fibers," *Appl. Phys. B* **54**(2), 175–180 (1992).
25. L. Gui et al., "Soliton molecules and multisoliton states in ultrafast fibre lasers: Intrinsic complexes in dissipative systems," *Appl. Sci.* **8**(2), 201 (2018).
26. Z. Q. Wang et al., "Optical soliton molecular complexes in a passively mode-locked fibre laser," *Nat. Commun.* **10**(1), 830 (2019).
27. D. Zou, Y. Zhang, Y. Song, and M. Hu, "Sub-100 fs Bound State Solitons and Period-Doubling Bifurcations in a Mode-Locked Fiber Laser," *IEEE Photonics Technol. Lett.* **32**(20), 1311–1314 (2020).
28. Y. Zhou et al., "Buildup and dissociation dynamics of dissipative optical soliton molecules," *Optica* **7**(8), 965–972 (2020).
29. A. Andrianov and A. Kim, "Widely stretchable soliton crystals in a passively mode-locked fiber laser," *Opt. Express* **29**(16), 25202–25216 (2021).
30. D. Y. Tang, L. M. Zhao, B. Zhao, and A. Q. Liu, "Mechanism of multisoliton formation and soliton energy quantization in passively mode-locked fiber lasers," *Phys. Rev. A* **72**(4), 043816 (2005).
31. S. R. Friberg, "Soliton fusion and steering by the simultaneous launch of two different-color solitons," *Opt. Lett.* **16**(19), 1484–1486 (1991).
32. M. Mitchell, M. Segev, and D. N. Christodoulides, "Observation of Multihump Multimode

- Solitons,” *Phys. Rev. Lett.* **80**(21), 4657 (1998).
33. D. N. Christodoulides, “Black and white vector solitons in weakly birefringent optical fibers,” *Phys. Lett. A* **132**(8–9), 451–452 (1988).
 34. J. P. Lourdesamy et al., “Spectrally periodic pulses for enhancement of optical nonlinear effects,” *Nat. Phys.* **18**59–66 (2022).
 35. O. Melchert et al., “Soliton Molecules with Two Frequencies,” *Phys. Rev. Lett.* **123**(24), 243905 (2019).
 36. D. Mao et al., “Synchronized multi-wavelength soliton fiber laser via intracavity group delay modulation,” *Nat. Commun.* **12**(1), 6712 (2021).
 37. R. Liao et al., “Dual-comb generation from a single laser source: principles and spectroscopic applications towards mid-IR—A review,” *J. Phys. Photonics* **2**(4), 042006 (2020).
 38. Y. Cui and X. Liu, “Graphene and nanotube mode-locked fiber laser emitting dissipative and conventional solitons,” *Opt. Express* **21**(16), 18969–18974 (2013).
 39. A. Krajewska et al., “Simultaneous mode-locking at 1565 nm and 1944 nm in fiber laser based on common graphene saturable absorber,” *Opt. Express* **21**(16), 18994–19002 (2013).
 40. C.-H. Chang, C.-P. Cheng, W.-W. Hsiang, and Y. Lai, “Passive synchronization between a self-similar pulse and a bound-soliton bunch in a two-color mode-locked fiber laser,” *Opt. Lett.* **34**(13), 1967–1969 (2009).
 41. R. K. Shelton et al., “Phase-coherent optical pulse synthesis from separate femtosecond lasers,” *Science* **293**(5533), 1286–1289 (2001).
 42. A. Mahjoubfar et al., “Time stretch and its applications,” *Nat. Photon.* **11**(6), 341–351 (2017).
 43. Y. Wei et al., “Ultrafast spectral dynamics of dual-color-soliton intracavity collision in a mode-locked fiber laser,” *Appl. Phys. Lett.* **112**(8), 081104 (2018).
 44. Y. Wang et al., “Universal mechanism for the binding of temporal cavity solitons,” *Optica* **4**(8), 855–863 (2017).
 45. C. Dorrer and I. A. Walmsley, “Characterization of ultrashort electromagnetic pulses,” *Adv. Opt. Photonics* **1**(2), 308–437 (2009).
 46. T. Xian, L. Zhan, W. Wang, and W. Zhang, “Subharmonic Entrainment Breather Solitons in Ultrafast Lasers,” *Phys. Rev. Lett.* **125**(16), 163901 (2020).
 47. J. M. Soto-Crespo, M. Grapinet, P. Grelu, and N. Akhmediev, “Bifurcations and multiple-period soliton pulsations in a passively mode-locked fiber laser,” *Phys. Rev. E* **70**(6), 066612 (2004).
 48. Z. W. Wei et al., “Pulsating soliton with chaotic behavior in a fiber laser,” *Opt. Lett.* **43**(24), 5965–5968 (2018).
 49. T. G. Philbin et al., “Fiber-optical analog of the event horizon,” *Science* **319**(5868), 1367–1370 (2008).
 50. Y. Cui et al., “XPM-Induced Vector Asymmetrical Soliton with Spectral Period Doubling in Mode-Locked Fiber Laser,” *Laser Photon. Rev.* **15**(3), 2000216 (2021).